Int. J. Electrochem. Sci., 16 **(2021)** Article ID: 210711, doi: 10.20964/2021.07.16

International Journal of
ELECTROCHEMICAL
SCIENCE
www.electrochemsci.org

Electrochemical Nonenzymatic Sensor Based on $NiOFe_2O_3$@carbon Nanotubes Nanocomposite for Determination of Paraoxon in Fruits and Water

Xiaoping Zhang[1], *Yingjie Feng*[2], *Jianhua Li*[3], *Dan Ai*[2], *Gaolei Xi*[2,*], *Mingqin Zhao*[1,*]

[1] College of Tobacco Science，Flavors and Fragrance Engineering & Technology Research Center of Henan Province, Henan Agricultural University, Zhengzhou 450002, China
[2] Technology Center, China Tobacco Henan Industrial Co., Ltd., Zhengzhou 450016, Henan, China
[3] Xuchang City Branch of Henan Tobacco Company, Xuchang 461000, Henan, China
[*]E-mail:zhaomingqinhau@sina.com

Received: 25 February 2021/ *Accepted:* 15 April 2021 / *Published:* 31 May 2021

Here, the $NiOFe_2O_3$@CNTs nanocomposite modified glassy carbon electrode ($NiOFe_2O_3$@CNTs/GCE) as nonenzymatic sensor was prepared for electrochemical determination of paraoxon in agricultural wastewater and apple juice. The sol–gel technique was used to synthesize the prepared nanocomposite. The structural and morphological characterizations of the nanocomposite were done by XRD and SEM analyses. The structural results showed that $NiOFe_2O_3$@CNTs/GCE composite has a high purity and great crystallinity with face-centered cubic structure of NiO nanoparticles (NiO NPs) and γ-Fe_2O_3nanoparticles (Fe_2O_3 NPs) which well distributed on the walls of CNTs. Electrochemical studies were done by voltammetry and amperometry techniques which exhibited that the synergistic effect of CNTs, NiO and Fe_2O_3 NPs in the nanocomposite can improved the electron transfer properties and electrocatalytic response of the nanocomposite to paraoxon. The limit of detection, sensitivity and linear range were obtained of 0.001 µM, 0.22246 µA/ µM and 10 to 220 µM, respectively. Applied studies on the paraoxon sensor for determination of paraoxon in prepared real samples showed the good accuracy and acceptable values of recovery and RSD. Thus, the proposed sensor can be reliable and effective for the determination of paraoxon in real samples.

Keywords: $NiOFe_2O_3$@CNTs; Nanocomposite; Paraoxon; Nonenzymatic sensor; Agricultural wastewater; Amperometry

1. INTRODUCTION

Organophosphate pesticides are designed to control insects and used in agriculture to control weeds, insect infestation and diseases [1]. Paraoxon (diethyl 4-nitrophenyl phosphate) as an organophosphate oxon is a synthetic aryl dialkyl phosphate compound [2]. It belongs to the class of organic compounds known as nitrobenzenes which contain a nitrobenzene moiety that consists of a benzene ring with a carbon bearing a nitro group [3]. It acts as organophosphate acetylcholinesterase inhibitor that is the bioactive metabolite of the insecticide parathion and is used as a pesticide[4-6].

Paraoxon as acetylcholinesterase inhibitor or cholinesterase inhibitor can inhibit the enzyme from breaking down the neurotransmitter acetylcholine into choline and acetate [7]. Thus, it increases enzyme level and duration of the neurotransmitter action. Therefore, it leads to an increase in the level of autonomic ganglia and neuromuscular junctions as acetylcholine receptors in the central nervous system [8, 9]. It is also used as an ophthalmological drug to treat glaucoma and postural tachycardia syndrome. Nevertheless, it has been observed actions on the parasympathetic nervous system may cause some health effects such as collapse, coma, hypoglycemia, muscle cramp, muscle weakness, fatigue, tremor, headache, depression, miosis, impairment of visual acuity, anxiety, respiratory difficulty, pulmonary edema, cyanosis, vomiting and heart block. This chemical component is readily absorbed through the skin [10].

Therefore, many studies have been conducted to detect of paraoxon from fruits, industrial and agricultural wastewaters through the enzymatic and nonenzymatic sensors [11-17]. The enzymatic biosensors have been shown the advantages of enhanced sensitivity, selectivity and low detection limit compared with the non-enzymatic sensors [18]. However, some intrinsic drawbacks of enzymes, for example high fabrication and storage cost, poor stability in alkaline and acidic solutions, non-enzymatic sensors have been interested in recent research because of cost-effective fabrication, high stability, and higher linear range[19-21]. Moreover, the development of nanoscience has provided new opportunities to fabricate nanostructured sensors [19, 20, 22-25]. Furthermore, advantages of nanostructured metal oxides such as high stability, low cost and easy production make them as the suitable material for fabrication of nanostructured non-enzymatic sensors [26-28]. Therefore, this study was conducted on synthesis of $NiOFe_2O_3$@CNTs nanocomposite modified GCE as a nonenzymatic sensor for electrochemical determination of paraoxon in fruits and water.

2. EXPERIMENT

NiO NPs, Fe_2O_3 NPs, $NiOFe_2O_3$ NPs, NiO@CNTs, Fe_2O_3@CNTs and $NiOFe_2O_3$@CNTs nanocomposites were synthesized using sol–gel method [29, 30]. Prior to the synthesis, the GCE was polished with 0.3 and 0.05 µm alumina slurry (95%, Hunan Jia Only New Energy Technology Co. Ltd., China) on microcloth pads for 20 minutes and washed ultrasonically with deionized water and ethanol (96%, Shandong Kawah Oils Co., Ltd., China), respectively. 1g CNTs (96%, length of 5-20µm, out diameter of 30-60nm, Xuzhou Jiechuang New Material Technology Co., Ltd., China) were purified and functionalized mixture of 0.5M nitric acid (65 wt %, Xilong Scientific Co., Ltd., China) and 0.5M sulfuric acid (98%, Xilong Scientific Co., Ltd., China) in volume ratio of 1:3 for 7 minutes. The functionalized CNTs were filtered (5.0 µm, Durapore® Membrane Filter) and rinsed with deionized water and ethanol, respectively. Then, 0.5 M $Ni(NO_3)_2 \cdot 6H_2O$ (≥98.5, Merck) and 1.0 M $Fe(NO_3)_2 \cdot 9H_2O$ (≥99.95%, Sigma-Aldrich) were ultrasonically added to the dispersed CNTs in ethanol. The obtained suspension was stirred for 24 hours at room temperature. The resulting product was transferred into the oven at 100°C for 12 hours to obtain the $NiOFe_2O_3$@CNTs nanocomposite. In order to remove any impurities, the $NiOFe_2O_3$@CNTs was calculated at 650°C in a furnace in the environment of argon for 3 hours. The calcined $NiOFe_2O_3$@CNTs was ultrasonically dispersed in 0.2 g/l dimethyl formamide (99.8%, Sigma-Aldrich). The cleaned GCE was dipped in suspension for 60 minutes. Then, GCE was dried at room temperature.

The scanning electron microscopy (SEM; Hitachi S-4800, Hitachi Ltd., Tokyo, Japan) and X-ray diffraction (XRD, RigakuMiniflex 600, Tokyo, Japan) with Cu Kα radiationwere used to characterization ofmorphology and structures of prepared electrodes. Cyclic voltammetry (CV), differential pulse voltammetry (DPV) and amperometry techniques were employed to electrochemical measurements on AUTOLAB electrochemical system (MetrohmAutolab B. V., Utrecht, Netherlands) in conventional three-electrode cell which contained Ag/AgCl (3.0 M KCl) as reference electrode, a platinum wire as a counter electrode, and the prepared electrodes as working electrodes. 0.1 M PBS as electrochemical electrolyte was prepared from 0.1 M H_3PO_4 and 0.1M NaH_2PO_4. 1M KCl (99.0%, Sigma-Aldrich) containing 1mM $K_3[Fe(CN)_6]^{3-/4-}$ (≥99%,Sigma-Aldrich) and 0.1M phosphate buffer solutions (PBS) aqueous solutions were used as electrolyte.0.1 M PBS prepared from mixing solutions of 0.1 M NaH_2PO_4 (≥98%, Sigma-Aldrich) and 0.1 M Na_2HPO_4 (≥99.0%,Sigma-Aldrich)in equal volume ratio.

For preparation the real sample of fruit, fresh apple was washed with water, and sliced. Then, the apple juice was extracted. After then, the apple juice was filtered and centrifuged for 15 minutes at 1000 rpm. The obtained supernatant was used to prepare a 0.1M PBS solution. For preparation of the real sample of agricultural wastewater, the agricultural wastewater whiteout any purification was used for preparation of the 0.1M PBS solution. 0.05µM of paraoxon was sprayed onto both of the prepared real samples. Finally, the prepared real samples were stored in the refrigerator at 4°C for electrochemical measurements.

3. RESULTS AND DISCUSSION

Figure 1 shows SEM images of CNTs and $NiOFe_2O_3$@CNTs nanocomposite modified GCE.As seen for CNTs/GCE in Figure 1a, CNTs with average diameter of 50 nm and length of are 3µm homogeneously distributed on the surface of GCE. The SEM image of $NiOFe_2O_3$@CNTs in Figure 1b shows that $NiOFe_2O_4$ particles are well distributed on the walls of CNTs and also exhibits that the $NiOFe_2O_3$@CNTs nanocomposite completely covers the GCE surface.

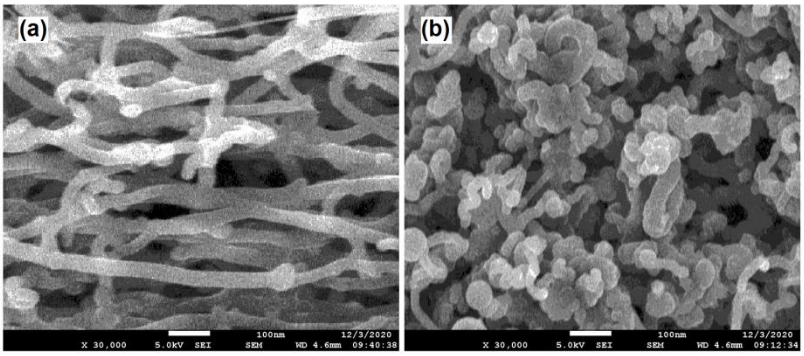

Figure1. SEM images of (a) CNTs and (b)$NiOFe_2O_3$@CNTs nanocomposite modified GCE.

XRD powder patterns of CNTs, NiO NPs, Fe_2O_3 NPs, $NiOFe_2O_3$ NPs, NiO@CNTs,Fe_2O_3@CNTs and $NiOFe_2O_3$@CNTs nanocomposite are shown in Figure 2. XRD pattern of CNTs powder in Figure 2a shows the two diffraction peaks at 2θ =26.10° and 42.98° that these peaks are ascribed to the graphite structure of the CNTs with (002) and (100) planes, respectively (JCPDS card no. 75–1621). As shown in Figures 2b and 2c,both XRD patterns of NiO NPs and NiO@CNTs with strong peaks at 37.39°, 43.55°, 62.92° and 75.12° for face-centered cubic structure of NiO with (111), (200),(220) and (311) planes (JCPDS Card. No. 78-0643). Moreover, XRD patterns of NiO@CNTs show typical (002) diffraction peaks of the graphite structure of CNTs at 26.06°, corresponding to composition of NiO and CNTs walls. Figures 2d and 2e show the diffraction patterns of Fe_2O_3 NPs and Fe_2O_3@CNTs with obvious peaks at 30.39°, 35.69°, 43.67°, 53.78°, 57.71° and 63.12° for phase of γ-Fe_2O_3 with (220), (311), (400), (422), (511) and (440) planes (JCPDS Card. No. 79-0418) [31]. The peak (002) plane in Figures 2e is also attributed with presence of CNTs in Fe_2O_3@CNTs nanocomposite. Figures 2f and 2g present the XRD patterns $NiOFe_2O_3$ NPs and $NiOFe_2O_3$@CNTs nanocomposite which contain the stronger diffraction peaks assigned to cubic NiO and Fe_2O_3, indicating that the final structure is a mixture of NiO and Fe_2O_3. In addition, $NiOFe_2O_3$@CNTs nanocomposite contains the (002) plane of CNTs which further confirms that the final product is of high purity and having great crystallinity.

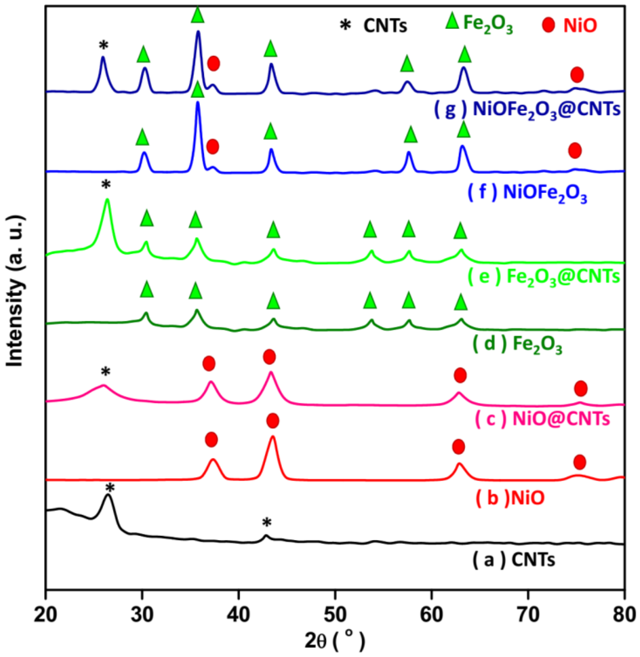

Figure 2. XRD powder patterns of (a) CNTs, (b) NiO NPs, (c) NiO@CNTs,(d) Fe_2O_3 NPs, (e) Fe_2O_3@CNTs, (f) $NiOFe_2O_3$ NPs and (g) $NiOFe_2O_3$@CNTs nanocomposite modified GCE.

Electrochemical responses of bare GCE and CNTs, NiO NPs, NiO@CNTs, Fe_2O_3 NPs, Fe_2O_3@CNTs, $NiOFe_2O_3$ NPs and $NiOFe_2O_3$@CNTs nanocomposite modified GCE in 1M KCl pH 7 containing 1mM $K_3[Fe(CN)_6]^{3-/4-}$ as redox probe was investigated at scan rate of 100 mV/s. Figure 3 depicts the CV curves of all electrodes with well-defined pairs of redox peaks ascribable to one electron transfer $(Fe(CN)_6)^{3-/4-}$ [32]. As observed, the peak-to-peak separation (ΔEp) of $(Fe(CN)_6)^{3-/4-}$ are 0.147, 0.144, 0.251, 0.230, 0.180, 0.133, 0.135 and 0.130V on the surfaces of bare GCE and CNTs, NiO NPs, NiO@CNTs, Fe_2O_3 NPs, Fe_2O_3@CNTs, $NiOFe_2O_3$ NPs and $NiOFe_2O_3$@CNTs nanocomposite modified GCE, respectively. Moreover, the observation on the peak currents reveals that CNTs, NiO, Fe_2O_3 and $NiOFe_2O_3$ NPs can enhance the peak current toward the bare GCE due to high porosity and specific surface area, and more electroactive sites of CNTs and metal oxide NPs on electrode surface [33]. ForNiO@CNTs/GCE and Fe_2O_3@CNTs/GCE, it is observed that CNTs can remarkably improve the conductivity and peak current, and the metal oxide NPs-coated CNTs are entangled with each other [34]. Thus, the interconnected structures of metal oxide NPs/CNTs not only enhanced the effective surface area of the electrode to facilitate rapid ion transfer/diffusion rates but also improved the electrons transfer because of the 3D conductive network of CNTs [35].Therefore, the higher peak current is occurred on $NiOFe_2O_3$@CNTs/GCE which attributed to the synergistic effect of CNTs, NiO and Fe_2O_3 NPs present in the nanocomposite [34, 35].Furthermore, decoration of NiO and Fe_2O_3 NPs on the surface of CNTs side walls improved the electron transfer properties of the nanocomposite and the anodic and cathodic peaks shift to lower potentials [34-36].

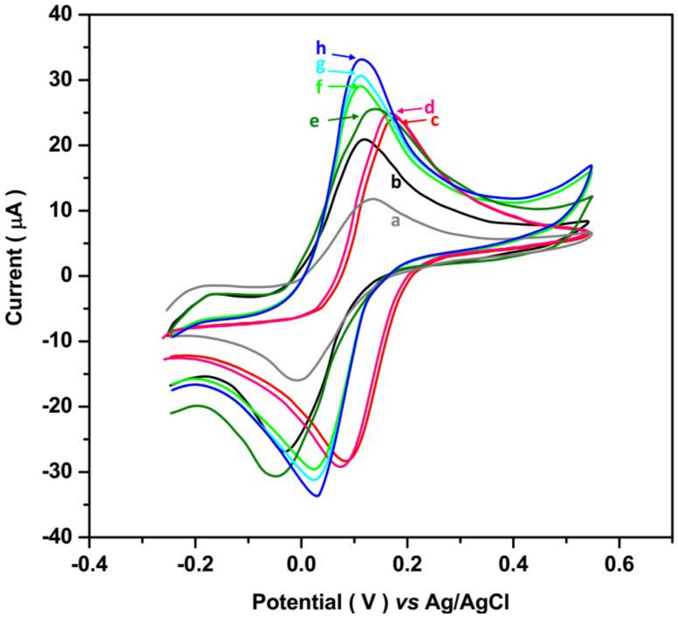

Figure 3. The CV curves of (a) bare GCE and (b) CNTs, (c) NiO NPs, (d) NiO@CNTs, (e) Fe_2O_3 NPs, (f) Fe_2O_3@CNTs, (g) $NiOFe_2O_3$ NPs and (h) $NiOFe_2O_3$@CNTs nanocomposite modified GCE in 1 M KCl pH 7 containing 1mM $K_3[Fe(CN)_6]^{3-/4-}$ at scan rate of 100 mV/s.

Further electrochemical measurements to study the electrocatalytic properties of the prepared electrodes in addition of 10μM and 20μM paraoxon solutions were carried out using the DPV technique in 0.1M PBS at 20 mV/s scan rate. The DPV curves in Figure 4 show that the reduction of paraoxon takes place at -0.56, -0.54, -0.55, -0.55, -0.54, -0.54, -0.52 and -0.51 V on the surfaces of bare GCE and CNTs, NiO NPs, NiO@CNTs, Fe_2O_3 NPs, Fe_2O_3@CNTs, $NiOFe_2O_3$ NPs and

$NiOFe_2O_3$@CNTs nanocomposite modified GCE, respectively, referring to the reduction of the nitro group and hydroxylamine formation [11]. The significant electrocatalytic response is obtained on $NiOFe_2O_3$@CNT/GCE because of its high and well-distributed electrocatalytic active sites of CNTs and metal oxide NPs for the paraoxon reduction which can achieve the fast electron-transfer kinetics between the electrode surface and the redox-active centers [37-39]. It is suggested that presence of the different nanostructured materials on hybrid structure of $NiOFe_2O_3$@CNT/GCE would also contribute to the increase in the sensitivity of the paraoxon electrochemical response [40]. Thus, the following electrochemical studies are conducted on $NiOFe_2O_3$@CNTs/GCE.

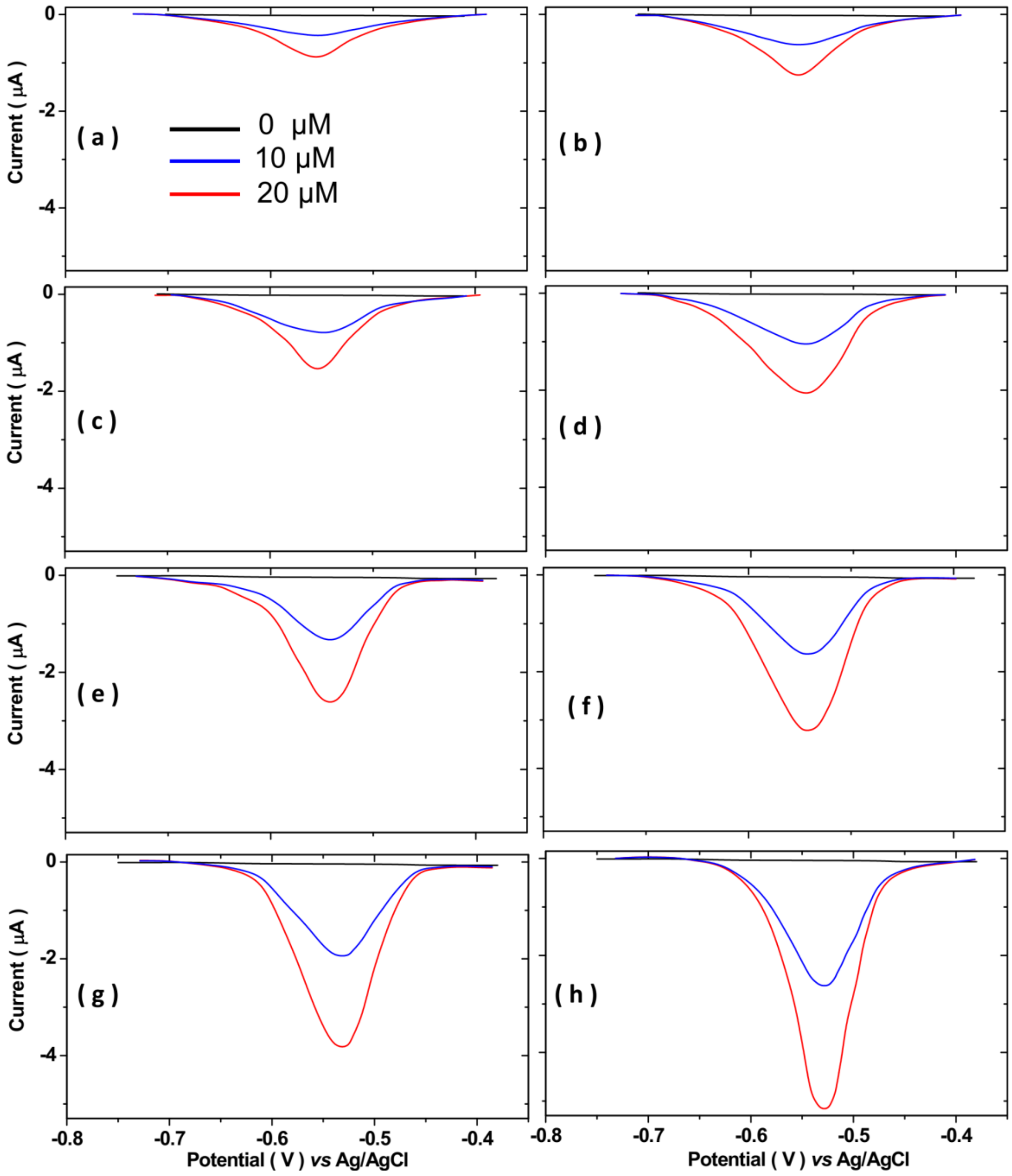

Figure 4. The DPV curves of (a) bare GCE and (b) NiO NPs, (c) Fe_2O_3 NPs, (d) $NiOFe_2O_3$ NPs, (e) CNTs, (f) NiO@CNTs, Fe_2O_3@CNTs and (g) $NiOFe_2O_3$@CNTs nanocomposite modified GCE in 0.1M PBS at 20 mV/s scan rate in additions 10µM and 20µM paraoxon solution.

The following electrochemical studies were performed using amperometry techniques to investigate the stability, detection limit, linear range, selectivity and applicability of paraoxon sensors. Figure 5 shows the obtained amperogram of NiOFe$_2$O$_3$@CNTs/GCE in 0.1 M PBS pH 7 at -0.50 V with addition of 10µM paraoxon. As observed, the electrocatalytic current is enhanced after injection of paraoxon. Moreover, the change electrocatalytic current of the electrode after 350 s of injection reveals 5% decrease, which indicated to stable response of NiOFe$_2$O$_3$@CNTs/GCE to determination of paraoxon because the NiOFe$_2$O$_4$ NPs prevent the fouling of electrode surface during the reaction [41].

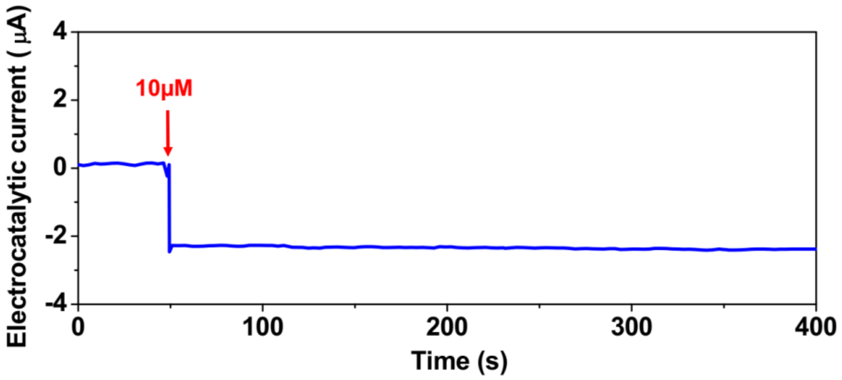

Figure 5. The obtained amperogramNiOFe$_2$O$_3$@CNTs/GCE in 0.1 M PBS pH 7 at -0.50 V with addition of 10µM paraoxon.

Figure 6 shows the obtained amperograms and calibration plot of NiOFe$_2$O$_3$@CNTs/GCE to successive injections of paraoxon in 0.1 M PBS pH 7 at -0.50 V. It is demonstrated to the fast responses of electrode to successive additions of 10µM paraoxon.

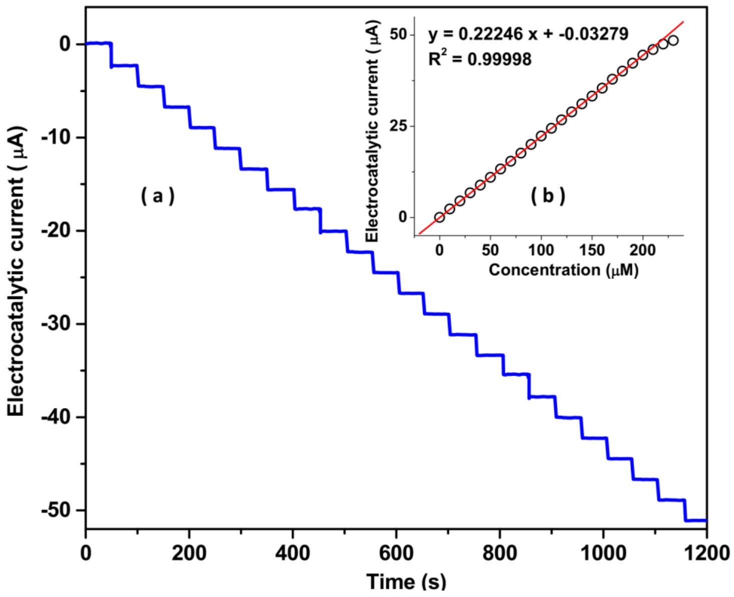

Figure 6. (a) The obtained amperogram and (b) calibration plot of NiOFe$_2$O$_3$@CNTs/GCE in 0.1 M PBS pH 7 at -0.50 V under successive injections of paraoxon.

Moreover, the limit of detection, sensitivity and linear range are obtained of 0.001 µM, 0.22246 µA/ µM and 10 to 220 µM, respectively. The obtained linear range and limit of detection of paraoxon using $NiOFe_2O_3$@CNTs/GCE are compared with the other reported paraoxon sensors in Table 1 which revealed to lower detection limit values and lower linear range for enzymatic biosensors than these in present study. By considering the higher chemical and mechanical stability of $NiOFe_2O_4$ NPs and CNTs toward the enzymatic biosensors, preferable properties of the magnetic nanoparticles and CNTs and great antifouling as well as the inherent catalytic capability of the nanoparticles [42], the $NiOFe_2O_3$@CNTs/GCE can be durable sensor for determination of paraoxon.

Table 1. A comparison study between NiOFe2O3@CNTs/GCE and other reported sensors for paraoxon determination

Electrode	**Technique**	**Linear Range (µM)**	**limit of detection (µM)**	**Ref.**
NiOFe2O3@CNT/GCE	AMP[a]	10 – 220	0.001	This work
Butyrylcholinesterase/PTTBO[b]/ graphite electrode	AMP	10–120	0.212	[12]
Imidazole/CNTs/ GCE	DPV[c]	1.0 - 16	0.12	[11]
TiO_2/ graphene oxide@UiO-66	SWV[d]	0.001–0.1	0.0002	[43]
acetylcholinesterase/cobalt phthalocyanine/screen printed carbon electrode	FI[e]	0.03-0.5	0.007	[13]
Cholinesterases/glass	FI	0.01 – 0.4	0.001	[44]
Acetylcholinesterase/ carbodiimide	FI	$5×10^{-5}$ – 0.001	$4 ×10^{-5}$	[45]
Acetylcholinesterase/MWCNTs /GCE	FI	$1 ×10^{-6}$–0.01	$4 ×10^{-7}$	[46]
PrussianBlue NPs/Butyrylcholinesterase /screen printed electrode	FI	0.007–0.04	0.004	[15]
Mg,Ncodoped Carbon dots	QUENCH[f]	0.005–3.0	$8.7×10^{-4}$	[47]
Acetylcholinesterase/ acetylthiocholine	QUENCH	$5.5 × 10^{-6}$ - $1.8 × 10^{-4}$	$3.5 × 10^{-6}$	[48]

[a] AMP:amperometry, [b] PTTBO:poly(5,6-bis(octyloxy)-4,7-di(thieno[3,2-b]thiophen-2 yl)benzo[c]oxoadiazole), [c] DPV: differential pulse voltammetry, [d] SWV: Squarewave voltammetry, [e] FI:Flow-injection, [f] QUENCH: quenchometry

In order to explore selectivity and anti-interference ability of prepared paraoxon sensor for practical application, the interference measurements using amperometry technique were carried out in existence of 10µM paraoxon and 50 µM possible interference like Br^-, Cu^{2+}, Ca^{2+}, Cl^-, SO_4^{2-}, and pesticides such as p-nitrophenol, chlorpyrifos methyl, ethyl-paraoxon, dimethoate, phoxim, fenitrothion, dichlofenthion, and parathion in 0.1 M PBS pH 7 at -0.50 V. Table 2 shows the obtained electrocatalytic currents of for interference substances is insufficient and ignorable toward the paraoxon recorded signal on $NiOFe_2O_3$@CNTs/GCE. Therefore, the substances in Table 2 do not interfere with paraoxon determination on $NiOFe_2O_3$@CNTs/GCE.

Table 2. (a) The obtained electrochatalytic current using amperometry technique on $NiOFe_2O_3$@CNTs/GCE to in 0.1 M PBS pH 7 at -0.50 V to injections 10 µM of paraoxon and 50 µM of interference substances.

Interfering substance	**Added (µM)**	**Electrocatalytic current response (µA)**	**RSD[a] (%)**
Paraoxon	10	2.280	±0.019
Br^-	50	0.021	±0.004
Cu^{2+}	50	0.025	±0.009
Ca^{2+}	50	0.026	±0.004
Cl^-	50	0.031	±0.009
SO_4^{2-}	50	0.029	±0.008
p-nitrophenol	50	0.042	±0.011
Chlorpyrifos methyl	50	0.033	±0.009
Ethyl-paraoxon	50	0.050	±0.010
Parathion	50	0.044	±0.015
Dichlofenthion	50	0.025	±0.009
Fenitrothion	50	0.052	±0.018
Phoxim	50	0.039	±0.012
Dimethoate	50	0.059	±0.017

[a]RSD: relative standard deviation

In order to consider the applicability of the paraoxon sensor in prepared real samples of agricultural wastewater and apple juice, the amperometry measurements were conducted on $NiOFe_2O_3$@CNTs/GCE to successive injections of paraoxon in 0.1 M PBS pH 7 at -0.50 V. Figure 8 shows the obtained calibration plots with good linearity. The paraoxon concentrations in prepared real samples of wastewater and apple juice are obtained 0.061 µM and 0.056 µM, respectively. Accordingly, the paraoxon contents in initial samples of apple and wastewater without any preparation steps are obtained 0.011 µM and 0.006 µM, respectively. In addition, to verify the applicability of the proposed paraoxon sensor, the analytical applicability of the $NiOFe_2O_3$@CNTs/GCE was studied to determine paraoxon in prepared real samples by standard addition technique. Table 3 represents the good accuracy of the obtained results with recovery values more than95.6% and RSD values lower than 4.25%. Thus, the prepared sensor may be reliable for the determination of paraoxon in fruits and water samples.

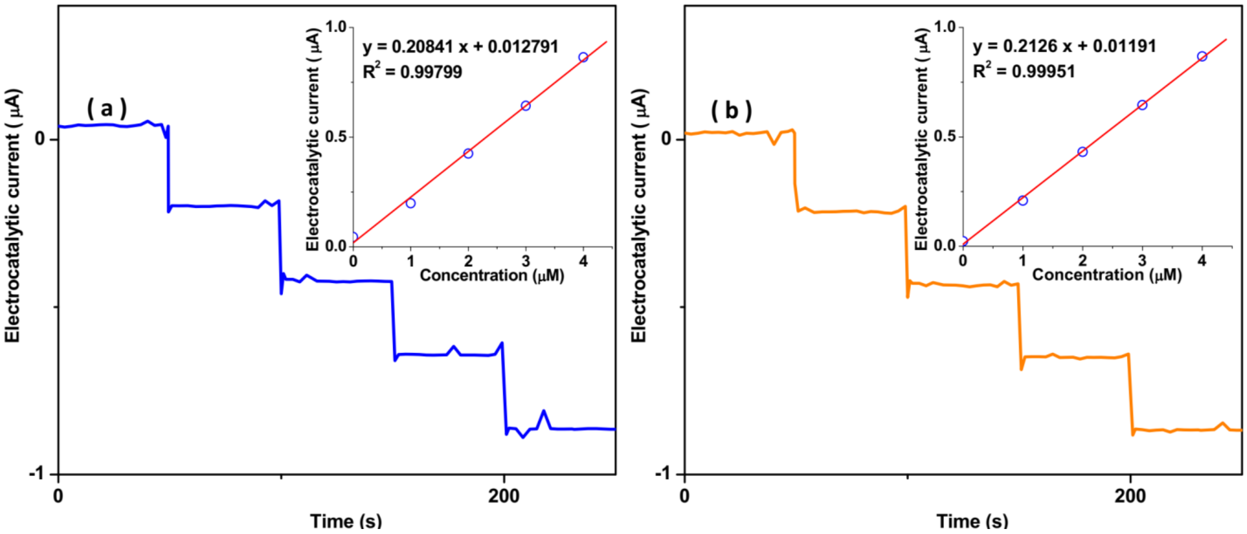

Figures 7. The obtained amperogram and calibration plot of NiOFe$_2$O$_3$@CNTs/GCE at -0.50 V under successive injections of paraoxon in prepared 0.1 M PBS pH 7 with real samples of (a) agricultural wastewater and (b) apple juice.

Table 3. Analytical results of NiOFe$_2$O$_3$@CNTs/GCE to determination paraoxon in prepared real samples of wastewater and apple (n=5).

Sample	**Added (µM)**	**Found (µM)**	**Recovery (%)**	**RSD (%)**
agricultural wastewater	1.00	0.99	99.0	4.11
	2.00	1.98	99.0	3.21
	3.00	2.87	95.6	3.55
	4.00	3.97	99.2	4.25
apple	1.00	0.97	97.5	2.01
	2.00	1.98	99.0	2.15
	3.00	2.96	98.6	3.18
	4.00	3.91	97.7	4.04

4. CONCULUSION

This study was focused on synthesis of NiOFe$_2$O$_3$@CNTs/GCE as an electrochemical nonenzymatic sensor for determination of paraoxon. The sol–gel method was applied to prepare NiOFe$_2$O$_3$@CNTs. The results of structural and morphological characterizations showed that NiO and

Fe_2O_4 particles were well distributed on the walls of CNTs which demonstrated an entangled network of functionalized CNTs with attached clusters of Ni and Fe. Results of electrochemical studies were revealed that the synergistic effect of CNTs, NiO and Fe_2O_3 NPs present in the nanocomposite improved the electron transfer properties of the nanocomposite. Moreover, the limit of detection, sensitivity and linear range were obtained of 0.001 µM, 0.22246 µA/ µM and 10 to 220 µM, respectively. The applicability of the paraoxon sensor was investigated in prepared real samples of agricultural wastewater and apple juice and results showed the good accuracy and recovery values more than 95.6% and RSD values lower than 4.25%. Thus, the prepared sensor may be reliable for the determination of paraoxon in fruits and water samples.

ACKNOWLEDGEMENT
This work was sponsored in part by Science and Technology Project of China National Tobacco Corporation Henan Tobacco Company (2018410000270095).

References

1. G. Wang, Y. Lan, H. Qi, P. Chen, A. Hewitt and Y. Han, *Pest Management Science*, 75 (2019) 1546.
2. C.M. Thompson, J.M. Gerdes and H.F. VanBrocklin, *Neurobiology of disease*, 133 (2020) 104455.
3. M.A.S. Oliveira, R.S.S. Oliveira and I. Borges, *Journal of Molecular Modeling*, 27 (2021) 1.
4. D.E. Lorke, S.M. Nurulain, M.Y. Hasan, K. Kuča and G.A. Petroianu, *Molecules*, 25 (2020) 1521.
5. H. Karimi-Maleh, M.L. Yola, N. Atar, Y. Orooji, F. Karimi, P.S. Kumar, J. Rouhi and M. Baghayeri, *Journal of colloid and interface science*, 592 (2021) 174.
6. S. Žunec, B. Radić, K. Kuča, K. Musilek and A.L. Vrdoljak, *Archives of Industrial Hygiene and Toxicology*, 66 (2015) 129.
7. J. Korram, L. Dewangan, I. Karbhal, R. Nagwanshi, S.K. Vaishanav, K.K. Ghosh and M.L. Satnami, *RSC Advances*, 10 (2020) 24190.
8. A. Vincent, *Neuroscience*, 439 (2020) 48.
9. H. Karimi-Maleh, M. Alizadeh, Y. Orooji, F. Karimi, M. Baghayeri, J. Rouhi, S. Tajik, H. Beitollahi, S. Agarwal and V.K. Gupta, *Industrial & Engineering Chemistry Research*, 60 (2021) 816.
10. G. Pozzessere, P. Rossi, E. Valle, C. Froio, A. Petrucci and C. Morocutti, *Clinical Autonomic Research*, 7 (1997) 315.
11. G.A. de Oliveira, A. Gevaerd, S.F. Blaskievicz, A.J.G. Zarbin, E.S. Orth, M.F. Bergamini and L.H. Marcolino-Junior, *Materials Science and Engineering: C*, 116 (2020) 111140.
12. J. Turan, M. Kesik, S. Soylemez, S. Goker, S. Coskun, H.E. Unalan and L. Toppare, *Sensors and Actuators B: Chemical*, 228 (2016) 278.
13. R.K. Mishra, R.B. Dominguez, S. Bhand, R. Muñoz and J.-L. Marty, *Biosensors and Bioelectronics*, 32 (2012) 56.
14. M. Pohanka, *International Journal of Electrochemical Science*, 11 (2016) 7440.
15. F. Arduini, D. Neagu, V. Scognamiglio, S. Patarino, D. Moscone and G. Palleschi, *Chemosensors*, 3 (2015) 129.
16. Z. Savari, S. Soltanian, A. Noorbakhsh, A. Salimi, M. Najafi and P. Servati, *Sensors and Actuators B: Chemical*, 176 (2013) 335.

17. H. Karimi-Maleh, S. Ranjbari, B. Tanhaei, A. Ayati, Y. Orooji, M. Alizadeh, F. Karimi, S. Salmanpour, J. Rouhi and M. Sillanpää, *Environmental Research*, 195 (2021) 110809.
18. W.-C. Lee, K.-B. Kim, N.G. Gurudatt, K.K. Hussain, C.S. Choi, D.-S. Park and Y.-B. Shim, *Biosensors and Bioelectronics*, 130 (2019) 48.
19. H. Zhu, L. Li, W. Zhou, Z. Shao and X. Chen, *Journal of Materials Chemistry B*, 4 (2016) 7333.
20. Z. Savari, S. Soltanian, A. Noorbakhsh and A. Salimi, *Electrochemical Society Iran*, 9 (2013) 1.
21. H. Karimi-Maleh, Y. Orooji, A. Ayati, S. Qanbari, B. Tanhaei, F. Karimi, M. Alizadeh, J. Rouhi, L. Fu and M. Sillanpää, *Journal of Molecular Liquids*, 329 (2021) 115062.
22. L. Wang, Y. Liu and Y. Chen, *International Journal of Electrochemical Science*, 16 (2021) 210464.
23. F. Chahshouri, H. Savaloni, E. Khani and R. Savari, *Journal of Micromechanics and Microengineering*, 30 (2020) 075001.
24. J. Rouhi, S. Kakooei, S.M. Sadeghzadeh, O. Rouhi and R. Karimzadeh, *Journal of Solid State Electrochemistry*, 24 (2020) 1599.
25. H. Savaloni, R. Savari and S. Abbasi, *Current Applied Physics*, 18 (2018) 869.
26. J. Wang, J. Wang, W. Li and C. Yang, *International Journal of Electrochemical Science*, 16 (2021) 210447.
27. R. Savari, H. Savaloni, S. Abbasi and F. Placido, *Sensors and Actuators B: Chemical*, 266 (2018) 620.
28. J. Rouhi, S. Kakooei, M.C. Ismail, R. Karimzadeh and M.R. Mahmood, *International Journal of Electrochemical Science*, 12 (2017) 9933.
29. Z. Sabouri, N. Fereydouni, A. Akbari, H.A. Hosseini, A. Hashemzadeh, M.S. Amiri, R. Kazemi Oskuee and M. Darroudi, *Rare Metals*, 39 (2020) 1134.
30. S.J. Davarpanah, R. Karimian and F. Piri, *Journal of Applied Biotechnology Reports*, 2 (2015) 207.
31. Z. Li, M. Peng, Y. Jin, X. Wang, Y. Cui and C. Chen, *Chinese Science Bulletin*, 56 (2011) 2911.
32. A.S. Adekunle, O.J. Fakayode, B.B. Mamba and T.T.I. Nkambule, *International Journal of Environmental Analytical Chemistry*, 1 (2020)
33. M. Mazloum-Ardakani, M. Maleki and A. Khoshroo, *Journal of Nanostructures*, 8 (2018) 350.
34. S. Zhang, X. Wang, Y. Li, X. Mu, Y. Zhang, J. Du, G. Liu, X. Hua, Y. Sheng and E. Xie, *Beilstein journal of nanotechnology*, 10 (2019) 1923.
35. E.G.B. Dassan, A.A. Ab Rahman, M.S.Z. Abidin and H.M. Akil, *Nanotechnology Reviews*, 9 (2020) 768.
36. Y. Mu, D. Jia, Y. He, Y. Miao and H.-L. Wu, *Biosensors and Bioelectronics*, 26 (2011) 2948.
37. S. Tajik, H. Beitollahi, F.G. Nejad, K.O. Kirlikovali, Q. Van Le, H.W. Jang, R.S. Varma, O.K. Farha and M. Shokouhimehr, *Crystal Growth & Design*, 20 (2020) 7034.
38. G. Valenti, A. Boni, M. Melchionna, M. Cargnello, L. Nasi, G. Bertoni, R.J. Gorte, M. Marcaccio, S. Rapino and M. Bonchio, *Nature communications*, 7 (2016) 1.
39. G.A. de Oliveira, A. Gevaerd, S.F. Blaskievicz, A.J. Zarbin, E.S. Orth, M.F. Bergamini and L.H. Marcolino-Junior, *Materials Science and Engineering: C*, 116 (2020) 111140.
40. N.M. Noah, *Journal of Nanomaterials*, 2020 (2020)
41. T. Aparna and R. Sivasubramanian, *J. Chem. Sci*, 130 (2018) 14.
42. A.A. Ensafi, B. Arashpour, B. Rezaei and A.R. Allafchian, *Materials Science and Engineering: C*, 39 (2014) 78.
43. N. Karimian, H. Fakhri, S. Amidi, A. Hajian, F. Arduini and H. Bagheri, *New Journal of Chemistry*, 43 (2019) 2600.
44. L. Pogačnik and M. Franko, *Talanta*, 54 (2001) 631.

45. J. J. Rippeth, T. D. Gibson, J. P. Hart, I. C. Hartley and G. Nelson, *Analyst*, 122 (1997) 1425.
46. G. Liu and Y. Lin, *Analytical Chemistry*, 78 (2006) 835.
47. J. Peng, W. Yin, J. Shi, X. Jin and G. Ni, *Microchimica Acta*, 186 (2018) 24.
48. K. Wang, L. Wang, W. Jiang and J. Hu, *Talanta*, 84 (2011) 400.